Desalination 404 (2017) 155–166

Contents lists available at ScienceDirect

Desalination

journal homepage: www.elsevier.com/locate/desal

Experimental investigation of the effect of electrospinning parameters on properties of superhydrophobic PDMS/PMMA membrane and its application in membrane distillation

Long-Fei Ren, Fan Xia, Jiahui Shao *, Xiaofan Zhang, Jun Li

School of Environmental Science and Engineering, Shanghai Jiao Tong University, 800 Dongchuan Road, Shanghai, 200240 Shanghai, PR China

HIGHLIGHTS

- Superhydrophobic PDMS/PMMA membrane was electrospun successfully with a contact angle of 163°.
- Correlations between electrospinning parameters and membrane properties were firstly established.
- Membrane surface roughness and beads structure were well-related with membrane hydrophobicity.
- The membrane was suitable for MD process (<24 h) with membrane flux of 39.61 L/m^2 h and salt rejection of 99.96%.

ARTICLE INFO

Article history:
Received 18 August 2016
Received in revised form 24 October 2016
Accepted 12 November 2016
Available online 16 November 2016

Keywords:
Electrospun membrane
PDMS
Superhydrophobic material
Water contact angle
Membrane distillation

ABSTRACT

Considerable efforts have been devoted to finding economic and simple preparation methods for polydimethylsiloxane (PDMS) superhydrophobic membrane in past decades. This study provides a simple method to electrospin PDMS membrane using poly (methyl methacrylate) (PMMA) as carrier polymer. Effects of PMMA concentration, PDMS/PMMA mass ratio and main parameters of electrospinning process (voltage and injection rate) were investigated to obtain superhydrophobic membrane with high water contact angle (WCA). A highest WCA of 163° could be obtained on the membrane surface fabricated by electrospinning solution containing PDMS: PMMA: tetrahydrofuran (THF): *N*,*N*-dimethylformamide (DMF) (mass ratio 1: 1: 8.88: 9.48) under applied voltage of 11 kV and injection rate of 0.1 mm/min. The superhydrophobic PDMS/PMMA membrane was further applied in membrane distillation process for desalination, and a high permeation flux of 39.61 L/m^2 h and an excellent salt rejection of 99.96% were achieved during long-term MD process (24 h).

1. Introduction

Rising demands of superhydrophobic membrane applied for contamination prevention, water repellency, self-cleaning, anti-icing and anti-corrosion [1] drive the relevant research on the fabrication of superhydrophobic membrane, whose surface exhibits a water contact angle (WCA) greater than 150° [2]. A variety of techniques, such as electrospinning, sol-gel method, plasma treatment, lithography and phase separation are currently adopted to produce superhydrophobic membrane [3,4]. All these techniques are closely related to low surface energy materials, either fabricating superhydrophobic membrane from such materials [5] or modifying membrane into superhydrophobic membrane by such materials [6].

Compared to other mentioned techniques, electrospinning is an economic consistent fiber spinning process which produces fibers with diameters in the range of nanometer, submicrometer and micrometer. When a high electric force beyond critical voltage acting on polymeric solution surface, the surface tension is overcome to realize the slim charged liquid jet continuously [7]. The liquid jet firstly extends into jet length, then further stretches into conical spiral motion and whipping motion. Finally, slim fibers produced by elongated jet are gathered on the rotation disc to form flat membrane gradually with the evaporation of solvent. Numerous polymeric materials have been electrospun into continuous, uniform fibers [8,9]. Polydimethylsiloxane (PDMS), a kind of elastomeric material and superhydrophobic polymer [4], has been widely applied in the fabrication of superhydrophobic materials mainly by one-step laser etching method [10] and plasma treatment [11]. The properties of low surface energy, low surface density and strong water repellence make PDMS an effective material in organics extraction [12], catalysts supports [13] and contamination prevention [14].

Though PDMS material itself is suitable for making superhydrophobic membrane, it is quite difficult to be electrospun due to insufficient chain entanglements during electrospinning as a small molecular polymer [15,16]. In order to obtain electrospun PDMS

* Corresponding author.
E-mail address: jhshao@sjtu.edu.cn (J. Shao).

http://dx.doi.org/10.1016/j.desal.2016.11.023
0011-9164/

membrane, poly (methyl methacrylate) (PMMA) was added into the electrospinning solution as carrier polymer [15,16]. It is believed that these two blending polymers change the intrinsic characterization of the insufficient chain entanglements existing in single PDMS polymer. Macromolecule PMMA could be easily electrospun into continuous fibers, while fragmentary PDMS fibers are distributed around PMMA fibers irregularly. The covalent bonds are produced between PDMS and PMMA fibers and then electrospun PDMS/PMMA membrane is produced. Though PDMS/PMMA membrane was successfully electrospun, this PDMS/PMMA membrane was used for protein microarrays as substrates [15,16] and the effects of system parameters (e.g. polymer concentration, viscosity) and process parameters (e.g. voltage, injection rate) on membrane morphology and hydrophobicity were not studied. The morphology and hydrophobicity of the electrospun membrane have significant effects on its further applications [17]. Thus, it is necessary to investigate the effects of various parameters on the morphology and hydrophobicity of PDMS/PMMA membrane made by electrospinning.

Membrane distillation (MD) is a thermally-driven separation process, which is driven by the vapor pressure difference existing between the porous hydrophobic membrane surfaces [18]. Due to its low operating temperatures, less energy consumption, as well as 100% theoretical rejection of non-volatile solute, MD is considered to be a next-generation water desalination technique [19,20]. An ideal membrane for MD should exhibit a superhydrophobic surface to avoid pore wetting and a well-designed pore structure to enhance water flux [21]. Therefore, the PDMS/PMMA membrane with high porosity, tunable pore size and considerable wetting resistance could be a great candidate for its application in MD. To the best of our knowledge, there is no report on electrospun PDMS/PMMA membrane used in MD process in the open literature.

In this study, PDMS/PMMA superhydrophobic membranes were electrospun using electrospinning solution of different amounts of PDMS and PMMA under different electrospinning process parameters. The electrospun PDMS/PMMA membranes were characterized by goniometer, scanning electron microscope (SEM), 3D automatic optical profiler, X-ray photoelectron spectroscopy (XPS) and tensile testing machine. The objective of this study was to investigate the effect of electrospinning system parameters (PMMA concentration, PDMS/PMMA mass ratio) and process parameters (voltage, injection rate) on morphology and hydrophobicity of the electrospun PDMS/PMMA membrane. The lab-made electrospun PDMS/PMMA membrane was further applied for the desalination in membrane distillation process. To the best of our knowledge, this is the first attempt to investigate the effects of electrospinning parameters on properties of electrospun PDMS/PMMA membrane and apply it in membrane distillation for desalination.

2. Materials and methods

2.1. Preparation of electrospinning solution

Weighted PMMA (9.9×10^5 Da, Sigma Aldrich) was firstly dissolved in a mixed solvent of tetrahydrofuran (THF) and *N*,*N*-dimethylformamide (DMF) by stirring 2 h (200 rpm, 50 °C). Then, weighted PDMS (Sylgard 184, Dow Corning) together with curing agent (10:1) was added by stirring 30 min (200 rpm, 25 °C). A LVDV-S rotary viscometer (Brookfield, USA) with S62 stirrer under a speed of 50 rpm was used to measure the viscosities of prepared electrospinning solutions at 25 °C. All the involved chemicals were from Sinopharm Chemical Reagent Co. Ltd. (Shanghai, China), otherwise being noted. They are of analytical grade and were directly applied in experiments without further purification.

2.2. Electrospinning of membrane

An integrated electrospinning machine (SS 20H, Ucalery, China) was used to fabricate the electrospinning solutions into micro-fibrous membranes under certain temperature (25 ± 3 °C) and humidity (35 ± 5%). The electrospinning solution was loaded into a 10 mL plastic syringe connecting 18# steel needle (0.86 mm inner diameter). Positive voltage was regulated as needed accompanied with a negative voltage of 1.00 kV. Different solution injection rates were tried and the electrospinning time was adjusted for consuming equal solution. The tip to collector distance (TCD) was maintained at 16 cm and the collector (50 rpm) was covered by tinfoil to receive the elongated fibers, which would further form membrane. After electrospinning process, the membranes were placed under 70 °C for 120 min to volatilize residual solvent and form cross-linking.

2.3. Characterization of membrane

2.3.1. Contact angle

The hydrophobicity of membrane surface was evaluated by WCA using Dropmeter A-200 contact angle system (MAIST Vision Inspection & Measurement Co., China) with corresponding Dropmeter software. Liquid droplet (9 μL) was dropped on at least five different points of each membrane for average and the algorithm of Young-Laplace was selected to analyze the contact angles above 90°.

2.3.2. Morphology

The morphologies of electrospun membranes were characterized by a scanning electron microscope (SEM, JSM - 6700F, JEOL, Japan). All samples (1 × 1 cm) were observed by SEM directly without coating gold layer as the electrical conductivity of membranes could satisfy the observational requirements. Averaged fiber diameters were calculated by corresponding SEM images. Pore sizes were measured using a 3H-2000PB membrane pore size analyzer (Beishide, China) by bubble-pressure method.

2.3.3. XPS analysis

X-ray photoelectron spectroscopy (XPS) spectra of membranes were recorded by a Kratos Axis Ultra^{DLD} spectrometer (Shimadzu-Kratos, Japan) with a monochromatic Al Kα radiation of 1486.6 eV. The analyzer was set to hybrid magnification mode under a take-off angle of 90°, while analysis area was about 700 × 300 μm under slot mode. Limited pressure of analysis chamber was set to $<5 \times 10^{-9}$ Torr. A binding energy (BE, 0–1200 eV) was used for wide spectrum scan, and corresponding X-ray source power was 75 W with a range of 75– 150 W for different elements in narrow spectrum scan. In addition, scanning steps and pass energies of 1 eV, 160 eV and 0.1 eV, 40 eV were employed

Table 1
Scheme of different PMMA concentrations and other parameters to electrospin membrane.

No.	Polymer p.			Solvent p.		Environmental p.		Electrospinning p.			
	PMMA (g)	PDMS (g)	PMMA c. (%)	THF (mL)	DMF (mL)	Temp (°C)	Humidity (%)	Voltage[a] (kV)	TCD[b] (cm)	Injection rate (mm/min)	Time (min)
M1-1	1	2	5.4	10	10	25 ± 3	35 ± 5	12	16	0.2	250
M1-2	2	2	10.9	10	10	25 ± 3	35 ± 5	13	16	0.2	250
M1-3	3	2	16.3	10	10	25 ± 3	35 ± 5	13	16	0.2	250

[a] The employed positive voltage was the minimum value to electrospin membrane steadily, while the negative voltage was set to 1.00 kV.
[b] The distance from the needle tip to collector.

in wide spectrum scan and narrow spectrum scan, respectively. The BE shifting of each element was calibrated by C1 s peak on 284.8 eV of sample surface. All samples were processed by the build-in Kratos charge neutralizer system to avoid the influence of charge effect.

2.3.4. Roughness

Surface profile and roughness of electrospun membranes were given by a 3D automatic optical profiler (ZeGage, ZygoLamda, USA) with a 50× camera lens. Three 2 × 2 cm samples taken from different locations of each membrane were employed to average the roughness of membrane surface, mainly by two amplitude metrics: roughness average (S_a) and root mean square roughness (S_q). S_a is the averaged roughness of the sample area (167 × 167 μm), and S_q is the mean square root of surface roughness for characterizing the surface roughness deviation. The scan scope of 50.0 μm was set to the center position mode while the signal thresh was set to 0.2%.

2.3.5. Thickness

Thickness of each membrane was measured using a membrane thickness gauge (Ch-12.7-JSM-6700F, Liuling, China). Five measurements at different position of each membrane were performed to obtain a mean value for better representation of thickness.

2.3.6. Tensile strength

Membrane mechanical properties of tensile strength (kPa), limiting stress (N) and elongation at break (%) were obtained with an electronic universal testing machine (6020, Zwick/Roell, Germany). Membranes were cut into a rectangle shape (70 × 10 mm) and tested under 0.7 N pre-load and 10 mm/min crosshead speed.

2.4. Direct contact membrane distillation (DCMD) test

A direct contact membrane distillation (DCMD) apparatus is set up to evaluate the membrane performance for desalination. The electrospun membrane with an effective area of 9.6 cm^2 was fixed in the circle cell module supported by a water-permeable PET layer. This placed membrane divided the cell module into feed solution side (down) and permeate solution side (up). The feed solution (1.5 L) was 3.5 wt% NaCl solution prepared in purified water with a conductivity (C_f) of 66.5 mS/cm, while the permeate solution was 1.5 L of purified water with a conductivity (C_p) of 1.2– 1.8 μS/cm. Flow rates of 1.0 and 0.5 L/min were used for feed side and permeate side via two gear pumps during all MD experiments. The temperature of feed solution was maintained at 70 °C by heating bath and the permeate solution

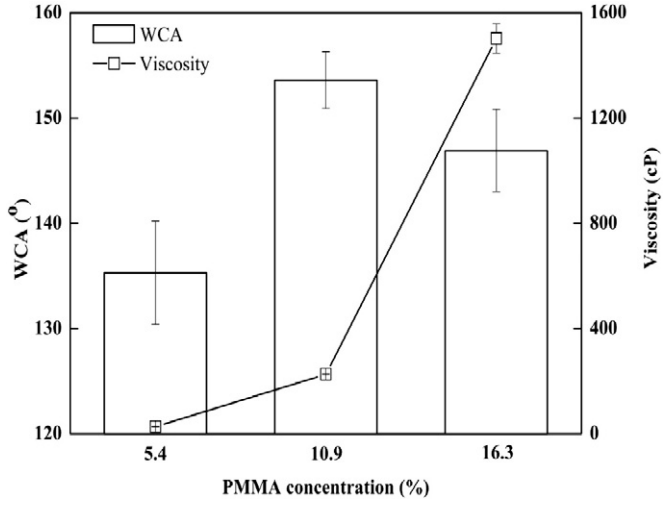

Fig. 1. Water contact angle (WCA) and viscosity of the electrospun membranes with PMMA concentrations of 5.4%, 10.9% and 16.3%.

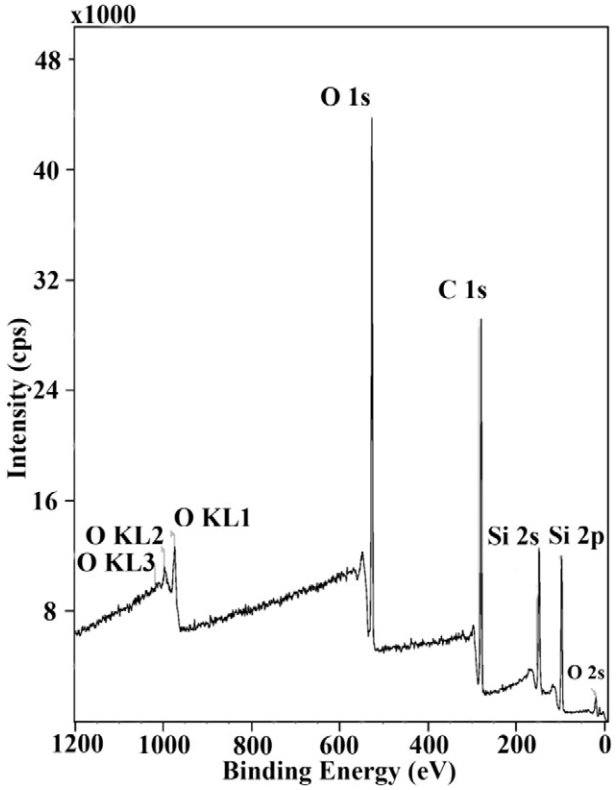

Fig. 2. XPS spectrum of M1-2 surface.

was maintained at 25 °C by a condenser. Weight of permeate tank was measured every 10 min by an electronic balance (YP10001, Guansen, China) to calculate membrane flux and conductivity of permeate solution was also recorded every 10 min by a conductivity meter (HI87314, HANNA, Italy) to calculate salt rejection. The liquid entry pressure (LEP) of membrane was determined following the method provided by another study [19]. Three frequently-used commercial membranes for DCMD were also employed in this MD process to compare their performances under same setup and conditions. They are PTFE membranes from Membrane Solutions MSPTFE022ETBX (MPTFE-1) and MSPTFE045ETBX (MPTFE-2), and PVDF membrane from Millipore (HVHP4700 (MPVDF)).

3. Results and discussions

3.1. Effect of system parameters on membrane properties

3.1.1. Effect of PMMA concentration

Table 1 provides detailed PMMA concentrations (M1-1: 5.4%, M1-2: 10.9% and M1-3: 16.3%) and other electrospinning parameters. A

Table 2
Scheme of different PDMS/PMMA mass ratios and properties of obtained membranes.

No.	Polymer p.			Electrospinning p.	Membrane p.	
	PDMS (g)	PMMA (g)	m_{PDMS}/m_{PMMA}	Voltage[a] (kV)	Fiber diameter (μm)	Pore size (μm)
M2-1	0	2	0/2	12		
M2-2	1	2	1/2	10	1.58 ± 0.30	9.15
M2-3	2	2	1/1	10	1.94 ± 0.54	7.70
M2-4	3	2	3/2	12	2.24 ± 0.47	11.90
M2-5	4	2	2/1	13	2.69 ± 0.82	13.43

[a] The employed positive voltage was the minimum value to electrospin membrane steadily, while the negative voltage was set to 1.00 kV. Other solvent, environmental and electrospinning parameters (not listed in Table 2) were the same as those listed in Table 1.

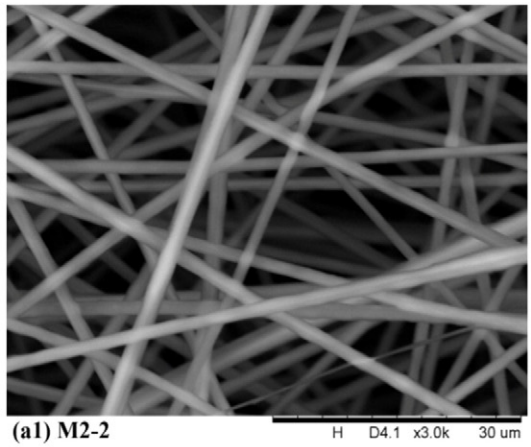

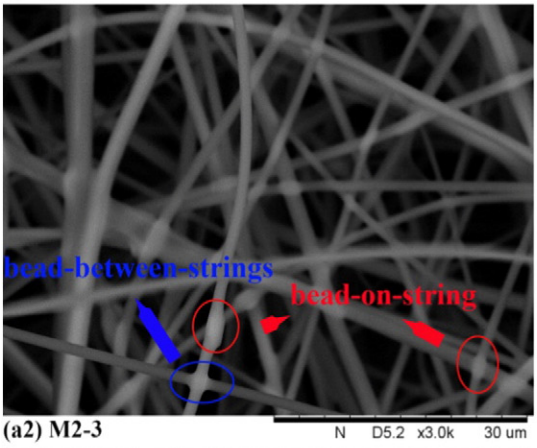

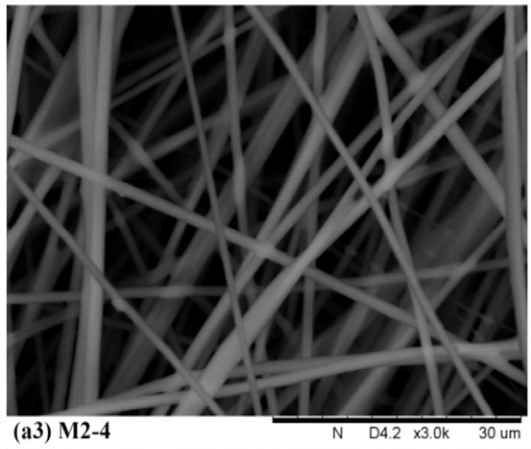

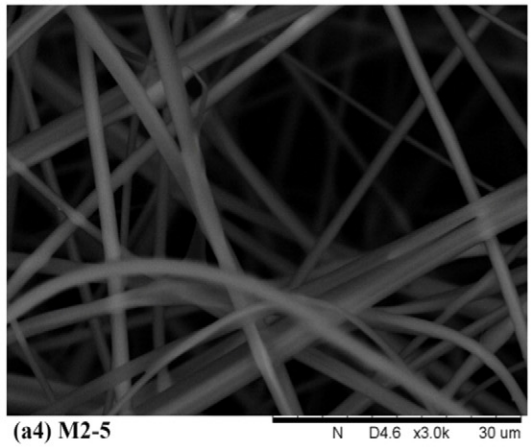

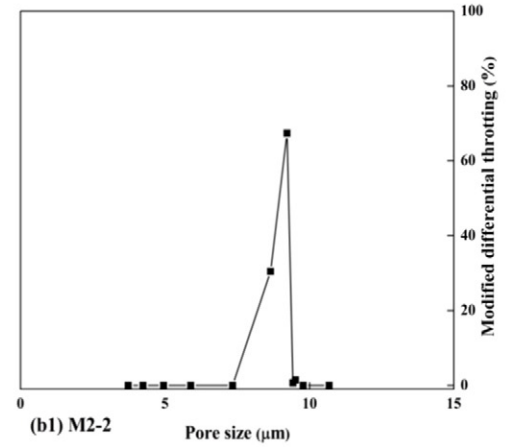

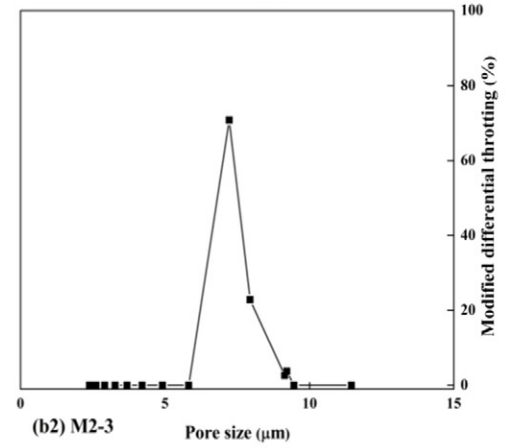

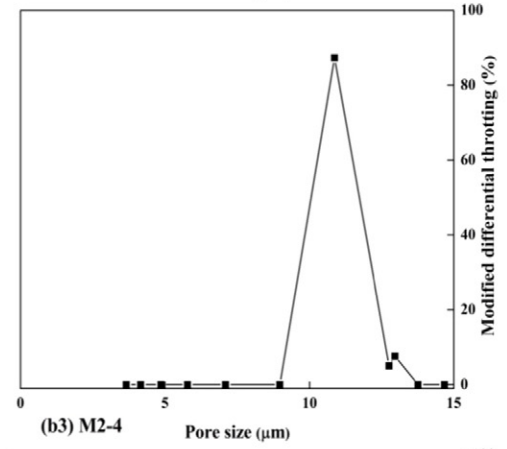

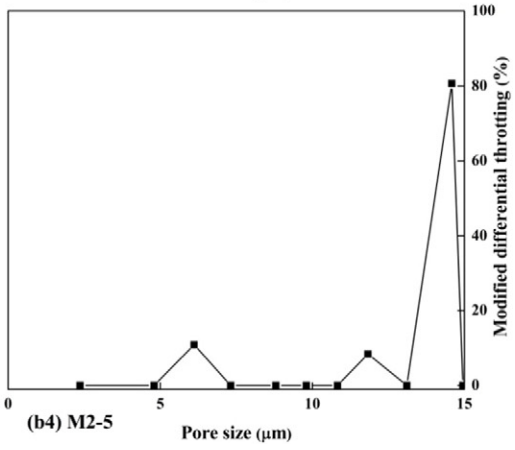

Fig. 3. (a) Surface SEM image and (b) pore size of membranes: (1) M2-2, (2) M2-3, (3) M2-4 and (4) M2-5.

mixture containing equal volumes of DMF and THF was employed as solvent system [22]. The solubility parameter (δ) of THF is about 9.5, which is close to that of PMMA (9.1–9.5) and PDMS (7.3–7.6), making THF a good solvent for both PMMA and PDMS. Though the δ value of co-solvent DMF (12.1) is not compatible with PMMA and PDMS, adding DMF could avoid excess solvent volatilization during electrospinning process.

Morphologies and thicknesses of three membranes with different PMMA concentrations are shown in Table S1. It is observed that membrane M1-1 (39.2 ± 3.2 μm) was quite thin compared to other two membranes, M1-3 (185.2 ± 9.9 μm) was too dense surrounding by quantities of flocs, and only M1-2 (71.2 ± 5.3 μm) possessed stable membrane structure accompanied with a few flocs. Therefore, the electrospinning solution with PMMA concentration of 10.9% is approved to be best choice for PDMS/PMMA membrane fabrication from the aspect of the membrane morphology. Fig. 1 shows the viscosities of electrospinning solution and the contact angles of electrospun membranes. With PMMA concentration increasing from 5.4% to 16.3%, the viscosity of electrospinning solution increased from 26.8 ± 1.2 cP (M1-1) to 1502.0 ± 55.7 cP (M1-3) dramatically. Similar trend was not seen in WCA on electrospun membrane surface. The WCA of membrane increased from 135.3 ± 4.9° for M1-1 with PMMA concentration of 5.4% to 153.6 ± 2.7° for M1-2 with PMMA concentration of 10.9%, and then declined to 146.9 ± 3.9° (M1-3) when PMMA concentration increased to 16.3%. Low PMMA dosage in M1-1 led to the low viscosity of electrospinning solution, which made fabricated M1-1 quite thin with large pore size (15.95 μm). Therefore, M1-1 was easier to be wetted and had a significant lower WCA in comparison with M1-1 and M1-2. Based on results of contact angle, the electrospinning solution with PMMA concentration of 10.9% could be considered as best condition for fabricating superhydrophobic membrane.

Fig. 2 shows XPS spectrum of M1-2 surface. It is observed that only elements carbon (C), oxygen (O) and silicon (Si) were detected when hydrogen (H) is not included as an immeasurable element in XPS analysis. The relative elemental composition was determined based on the intensity of the O (1 s, 2 s), Si (2 s, 2p) and C (1 s) peaks centered around 532.5 (1 s), 102.5 (2 p), and 284.8 eV, respectively. C was the most abundant element with an atom concentration of 54.0%, while the atom concentrations of O and Si were 25.9% and 20.1%, respectively. According to previous studies, the peaks of Si (2 s) and Si (2 p) belong to PDMS, and the peaks of O (1 s, 2 s), C (1 s) belong to both PDMS and PMMA [16,23,24]. Such elemental compositions provided clear evidence that the surface of M1-2 contained predominantly PMMA and PDMS and no chemical reaction happened between PDMS and PMMA during electrospinning. The intensity of C (1 s) peak was about 29,000 cps in 284.8 eV. This peak is generally related to the C—H bond of methyl groups, which is beneficial to the formation of highly hydrophobic membrane surface [25].

3.1.2. Effect of PDMS/PMMA mass ratio

Table 2 provides the details of different mass ratios of PDMS/PMMA (M2-1: 0/2, M2-2: 1/2, M2-3: 1/1, M2-4: 3/2, M2-5: 2/1) and the properties of the corresponding membranes. Fig. 3 shows the surface SEM images and pore size measurements of these membranes except M2-1 which failed in fabricating membrane. The surface tension of PMMA polymer (41 dynes/cm) was higher than that of PDMS/PMMA co-polymers (PDMS: 23 dynes/cm). Therefore, it is relatively difficult to overcome the surface tension of pure PMMA electrospinning solution to form fibers [26] and the corresponding electrospun product looked like a layer of spray/bead rather than membrane. SEM pictures in Fig. 3(a) and data in Table 2 indicate that fiber diameter increased with increasing PDMS/PMMA mass ratio. Smaller fiber diameters were observed for M2-2 (1.58 ± 0.30 μm) and M2-3 (1.94 ± 0.54 μm) and larger fiber diameters for M2-4 (2.24 ± 0.47 μm) and M2-5 (2.69 ± 0.82 μm). The relationship between PDMS/PMMA fiber diameter and PDMS/PMMA mass ratio is in agreement with the results reported by Yang et al. [16], which indicated that increasing PDMS/PMMA mass ratio would bring increasing fiber diameter. As depicted in Fig. 3(b), the pore size showed a rising tendency from 9.15 to 13.43 μm with increasing PDMS/PMMA mass ratio. However, the smallest pore size (7.70 μm) was detected on M2-3, rather than M2-2 with lowest PDMS/PMMA mass ratio.

It is also observed in Fig. 3(a) that only M2-3 exhibited bead-on-string structure with average bead size of 0.75 μm, which was probably caused by axisymmetric instabilities (Rayleigh instability and axisymmetric conducting instability) of dumbbell-like electrospun jets [27]. The other kind of bead (bead-between-strings) was also observed on the surface of M2-3. The roughness of each membrane was measured and detailed results are shown in Fig. S1. The roughness parameters of M2-3 were 6.7 μm (S_q) and 5.3 μm (S_a), which were 4.7–24.1% and 3.9–23.3% higher than those of other membranes (S_q and S_a of M2-2: 6.1, 4.9 μm; M2-4: 6.4, 5.1 μm; M2-5: 5.4, 4.3 μm). Therefore, it is reasonable to conclude that the surface of bead-rich membrane (M2-3) has higher roughness than that of bead-free membrane. The pore size of bead-rich membrane (M2-3, 7.70 μm) was also smaller than that of bead-free membranes (9.15–13.43 μm) due to the interception of beads. With higher roughness, the fiber arrangement on M2-3 surface was also more chaotic in comparison with other membranes as indicated in Fig. 3(a) and Fig. S1.

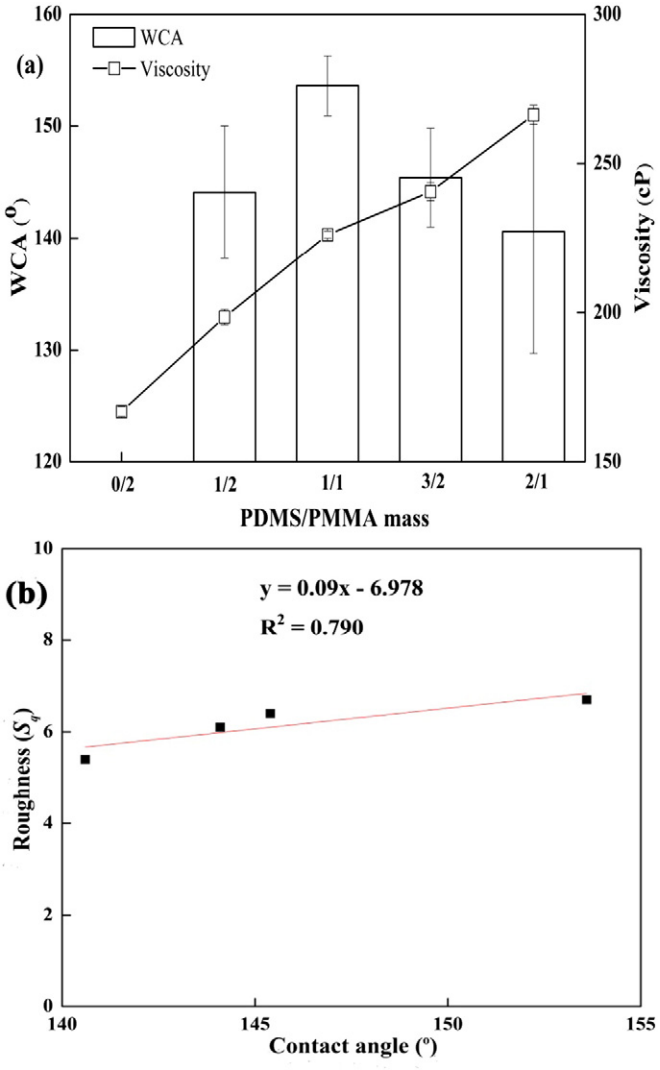

Fig. 4. (a) Corresponding variations between WCA and viscosity of four membranes, (b) correlation between contact angle and roughness (S_q).

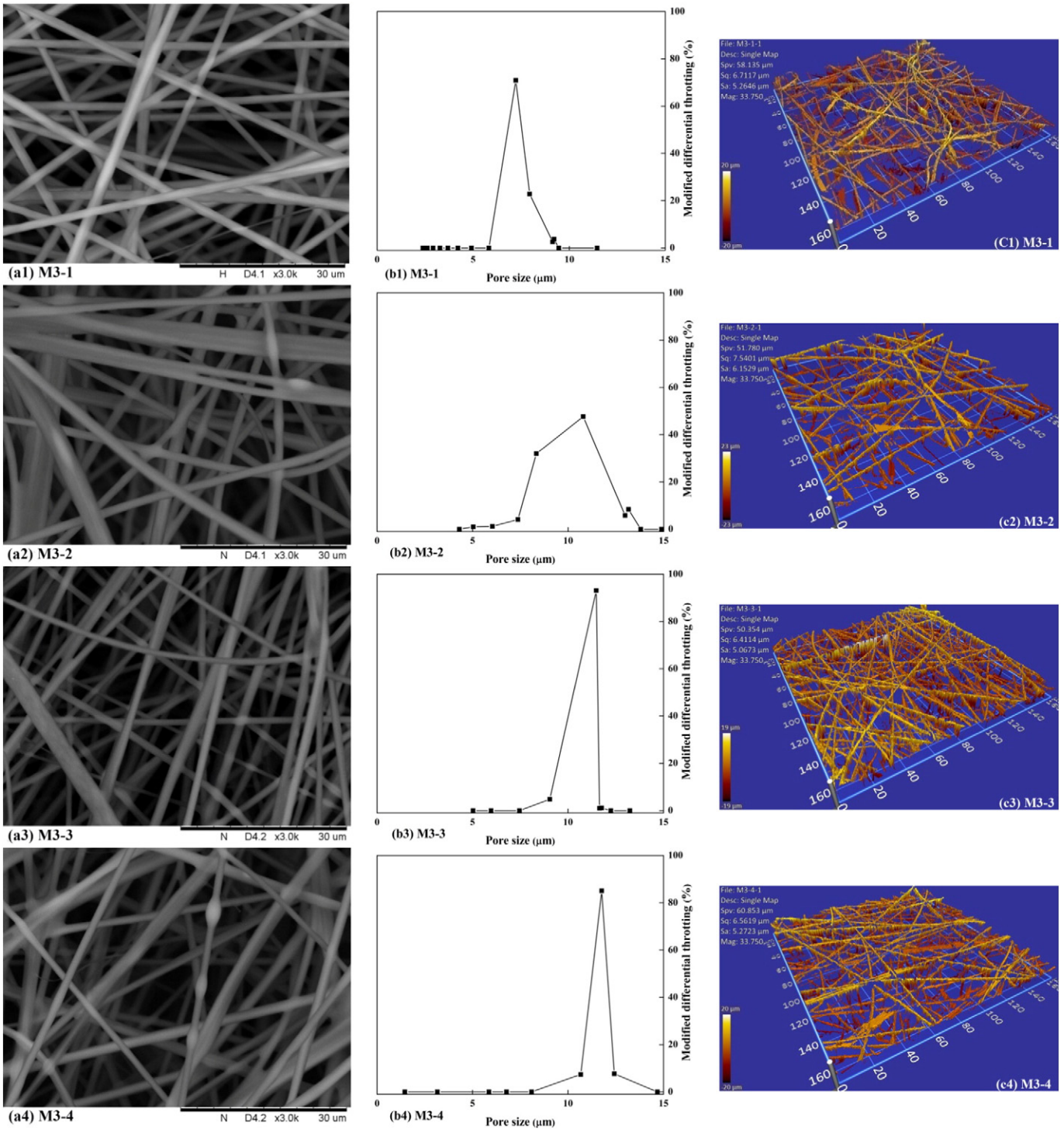

Fig. 5. (a) Surface SEM image, (b) pore size and (c) roughness of membranes: 05.

Table 3
Scheme of different voltages and properties of obtained membranes.

No.	Polymer p.	Electrospinning p.	Membrane p.	
	m_{PDMS}/m_{PMMA}	Voltage[a] (kV)	Fiber diameter (μm)	Pore size (μm)
M3-1	1/1	10	1.94 ± 0.54	7.70
M3-2	1/1	11	1.88 ± 0.38	11.34
M3-3	1/1	13	1.75 ± 0.79	11.50
M3-4	1/1	15	1.68 ± 0.54	11.73

[a] The negative voltage was set to 1.00 kV. Other solvent, environmental and electrospinning parameters (not listed in Table 3) were the same as those listed in Table 1.

Fig. 4(a) shows that the viscosity of electrospinning solution increased from 167.0 ± 1.7 cP for M2-1 to 266.2 ± 2.2 cP for M2-5 as PDMS/PMMA mass ratio increases from 0/1 to 2/1. The observation that PDMS/PMMA fiber diameter would increase with the increase of solution viscosity is also in agreement with Yang et al. [16]. In addition, Fig. 4(a) shows the WCA of the membranes with different PDMS/PMMA ratios. It is observed that WCA increased from 144.1 ± 5.9° for M2-2 to 153.6 ± 2.7° for M2-3 with the increase of PDMS/PMMA mass ratio. However, further increase of PDMS/PMMA mass ratio did not lead to higher WCA. WCA for M2-4 dropped to 145.4 ± 4.4° and further decreased to 140.6 ± 10.9° for

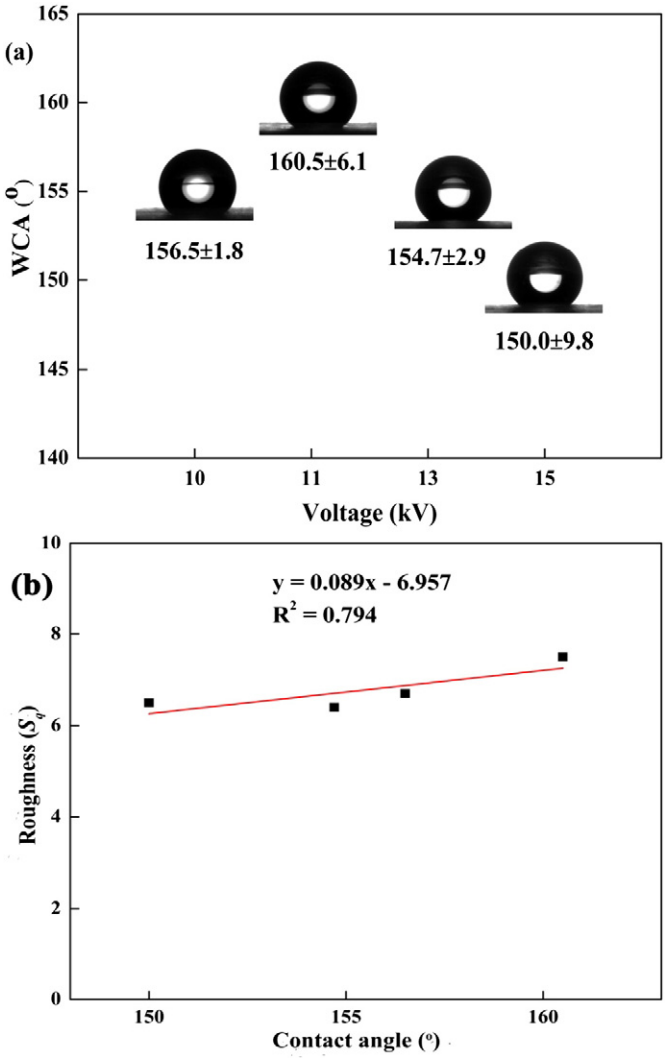

Fig. 6. (a) Corresponding variations between WCA and voltage of four membranes, (b) correlation between contact angle and roughness (S_q).

M2-5. The presence of beads was found to be beneficial to fabricate the membrane with high WCA in this study though usually being regarded as "by-products" in other electrospinning process [28]. The highest WCA and roughness were observed on M2-3, and the lowest WCA and roughness were observed on M2-5, which indicated that WCA of membrane probably is well related with its roughness. This is in agreement with Wenzel model, which believes that membrane with rougher surface is usually correlated well with more hydrophobic surface with higher WCA [29]. The morphology of membrane with high roughness seemed to be beneficial to receive high WCA by minimizing the valid contact area between water drop and membrane as it had been confirmed that membrane with high roughness would inhibit the migration of cells from surface into inner part by minimizing valid contact area [30].

It is concluded that the increase of PDMS/PMMA mass ratio lead to increased solution viscosity, which further caused the increase of fiber diameter and less beads formed. The formation of beads was found to be beneficial to obtain higher contact angle due to higher roughness and smaller pore size. The correlation between contact angle and roughness (S_q) was established with a correlation coefficient of about 0.790 (Fig. 4(b)). The optimum electrospinning solution for superhydrophobic membrane fabrication was a mixture of PDMS/PMMA/THF/DMF (1/1/8.88/9.48 calculated by mass), and this electrospinning solution was chosen in further experiments to investigate the effect of electrospinning process parameters.

3.2. Effect of process parameters on membrane properties

3.2.1. Effect of voltage

Fig. 5(a) shows the SEM images of PDMS/PMMA electrospun membranes obtained with different positive voltages of 10 kV (M3-1), 11 kV (M3-2), 13 kV (M3-3) and 15 kV (M3-4). The mean fiber diameter of these membranes decreased from 1.94 μm (M3-1) to 1.68 μm (M3-4, listed in Table 3) as the applied voltage increased from 10 kV to 15 kV. It is believed that when applied positive voltage increases, enhanced electrostatic force would act on electrospinning solution jet at needle tip to promote the solvent volatilization for the fiber formation with decreased diameter [7,31,32]. It is also observed that the number and size of beads reduced slightly with the increase of voltage. Higher voltage could promote whipping instability and inhibit axisymmetric instabilities, and then fiber with smaller bead would form under higher drawing stress at solution jet [27]. The membrane pore size was found to increase from 7.70 μm to 11.73 μm continuously with increasing applied voltage from 10 kV to 15 kV as shown in Fig. 5(b) and listed in Table 3. Therefore, it could be concluded that the increase of voltage could lead to the decrease of fiber diameter, bead formation and the increase of pore size.

In addition, Fig. 5(c) shows the surface roughness of these membranes. No obvious differences were observed for the roughness parameters of the membranes M3-1, M3-3 and M3-4 except M3-2 made with voltage of 11 kV. Its S_q was 7.5 μm, while the corresponding values for other membranes were about 6.4–6.7 μm. M3-2 also possessed the highest S_a value of 6.1 μm in contrast with low S_a values (5.1–5.3 μm) of other membranes, which indicated its surface containing more ups and downs than other membranes. Multilevel roughness in hierarchical structure of membrane is considered to be essential to approach extreme superhydrophobicity. When a 9 μL water droplet was placed on M3-2, an almost spherical droplet was observed and WCA of 160.5 ± 6.1° was measured as shown in Fig. 6(a). WCAs of other membranes were all below 157°: 156.5 ± 1.8° (M3-1), 154.7 ± 2.9° (M3-3) and 150.0 ± 9.8° (M3-4), indicating M3-2 is the most superhydrophobic membrane. A positive correlation between contact angle and roughness (S_q) was established with a correlation coefficient of about 0.794 (Fig. 6(b)). Based on WCA measurements, 11 kV seemed to be most suitable choice as positive voltage for electrospun under these parameters.

Table 4
Scheme of different injection rates and properties of obtained membranes.

No.	Polymer p.	Electrospinning p.			Membrane p.			
	m_{PDMS}/m_{PMMA}	Voltage[a] (kV)	Injection rate (mm/min)	Time (min)	Diameter (μm)	WCA (°)	Thickness (μm)	Pore size (μm)
M4-1	1/1	11	0.05	1000	1.28 ± 0.36	157.7 ± 4.3	29.6 ± 4.4	6.25
M4-2	1/1	11	0.1	500	1.75 ± 0.56	163.1 ± 3.5	65.4 ± 3.4	8.03
M4-3	1/1	11	0.2	250	1.88 ± 0.38	160.5 ± 6.1	79.2 ± 6.7	11.34
M4-4	1/1	11	0.5	100	2.89 ± 0.38	155.5 ± 2.1	125.0 ± 10.6	12.14

[a] The negative voltage was set to 1.00 kV. Other solvent, environmental and electrospinning parameters (not listed in Table 4) were the same as those listed in Table 1.

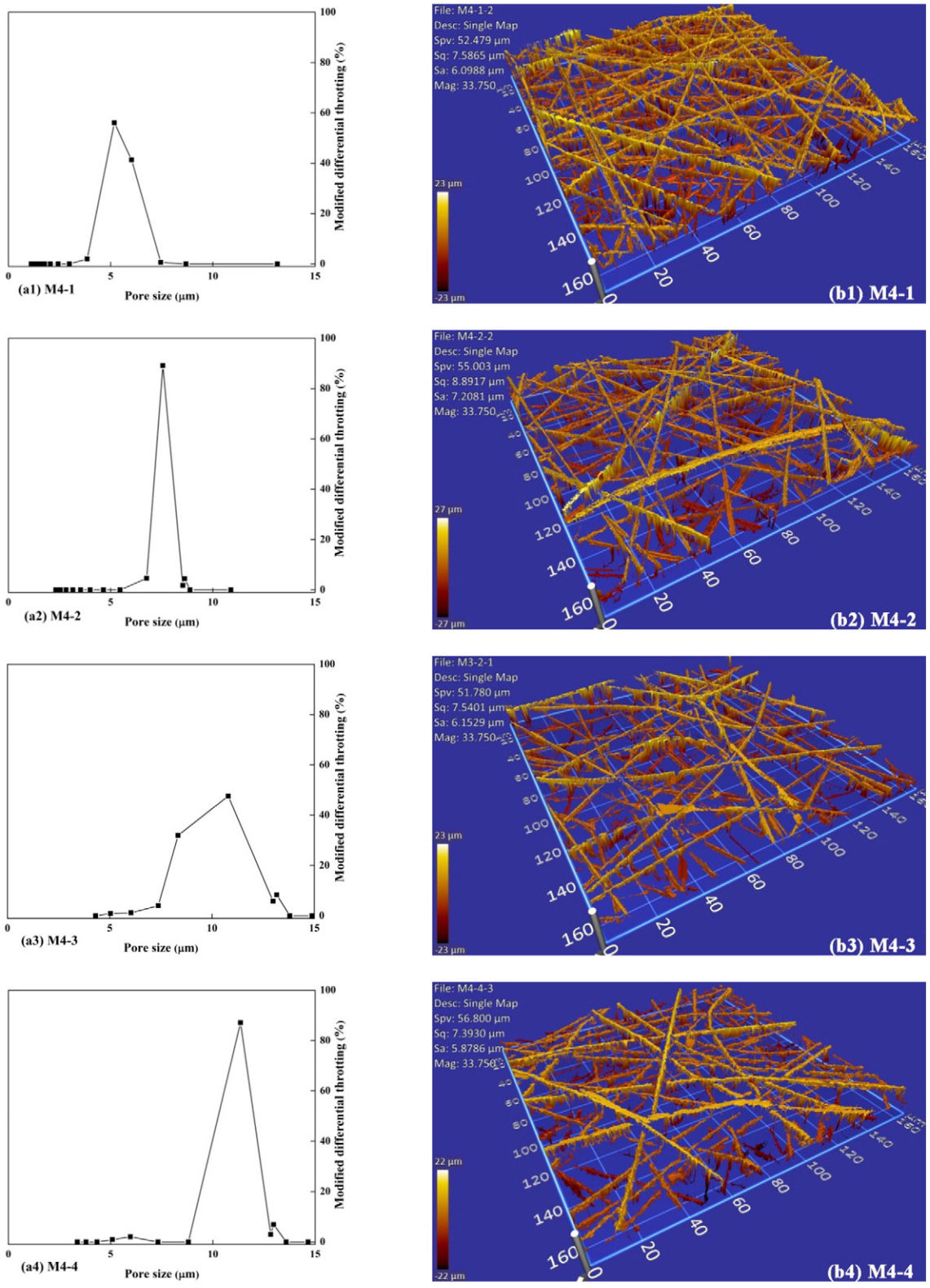

Fig. 7. (a) Pore size and (b) roughness of membranes: (1) M4-1, (2) M4-2, (3) M4-3 and (4) M4-4.

3.2.2. Effect of injection rate

Morphology of electrospun membrane is usually related to the injection rate to a great extent [33]. Selected injection rates of 0.05 mm/min (M4-1), 0.1 mm/min (M4-2), 0.2 mm/min (M4-3), 0.5 mm/min (M4-4) were employed for membrane optimization with other optimum conditions unchanged. Fig. S2 shows the morphologies of membranes made under different injection rates. The mean diameter of fibers was observed to increase from 1.28 μm for M4-1 to 2.89 μm for M4-4 with injection rate increasing from 0.05 mm/min to 0.5 mm/min (Table 4). The fiber diameter of M4-4 was much larger than diameters of other membranes and presented analogous silver ragwort leave structures, and numbers of hierarchical nano/micro-structure grooves were also

found on fibers. In addition, the thickness of membrane as shown in Table 4 increased from 29.6 ± 4.4 μm for M4-1 to 125.0 ± 10.6 μm for M4-4 when the injection rate increased from 0.05 to 0.5 mm/min with other parameters unchanged. The increase of injection rate also led to the increase of pore size from 6.25 μm for M4-1 to 12.14 μm for M4-4 (Fig. 7(a)). With the increase of injection rate, more electrospinning solution could be injected to needle tip within the same time. The superfluous solution jet is difficult to stretch sufficiently under the same electrostatic force and the solvent is difficult to evaporate sufficiently in the short electrospinning time. Therefore, higher injection rate would lead to the electrospun membrane with larger fiber diameter and thicker membrane eventually.

Fig. 7(b) shows the surface pictures by profilometer of these four membranes. A significantly higher roughness (S_q = 8.9 μm, S_a = 7.3 μm) was detected on the M4-2 surface than those of other membranes. The WCA (listed in Table 4) of the M4-2 was found to be 163.1 ± 3.5°, whereas that for other membranes was 157.6 ± 4.3° (M4-1), 160.5 ± 6.1° (M4-3) and 155.5 ± 2.1° (M4-4) respectively, which indicates roughness is well-related with hydrophobicity. It is further observed that M4-2 owned the most and largest beads, while the formed beads on other membranes were relatively fewer and smaller. These results revealed that bead-rich membrane was likely to generate rougher surface and larger WCA than the bead-less membrane.

In summary, the optimum electrospinning parameters were chosen as follows to provide the membrane most hydrophobic property: TCD of 16 cm, voltage of 11 kV, injection rate of 0.1 mm/min with electrospinning environmental parameters of temperature 25 °C and humidity 35%. The electrospun membrane under this condition (M4-2) was also used in the further mechanical test and membrane distillation.

3.3. Mechanical property

The stress-elongation curve together with surface morphology of M4-2 is presented in Fig. 8. This curve indicated that M4-2 belonged to homogeneous-plastic material. The entire elongation stage of M4-2 were divided into elastic phase, yield stage, extensional phase and necking stage according to the phases of normal plastic material. Table 5 provides the corresponding mechanical properties of limiting stress, tensile strength and elongation at break of M4-2. In the end of elastic phase (just before the peak of the curve), the force increased rapidly to a limiting force of 1.19 N assuming the force area is unchanged. The stress for M4-2 increased to 1833.89 kPa at the end of yield phase (just after the peak of the curve). Most of M4-2 fibers began to break at elongation of 25%, causing the huge decrease of stress as presented in Fig. 8. This huge decrease indicated the beginning of extensional phase. Then, the stress for M4-2 decreased dramatically to about 700 kPa in extensional phase and valley of stress-elongation curve indicated the end of extensional phase and the beginning of necking phase. All fibers of M4-2 were broken at elongation of 58.72% at the end of necking phase. These properties indicated that M4-2 was deformed easily and this was also the reason for using a water-permeable PET layer as supporting layer in the following MD process.

3.3.1. Short-term membrane distillation performance

Fig. 9 shows the direct contact membrane distillation apparatus (a) and corresponding membrane distillation performances for M4-2 and three commercial membranes during 360 min (b). Relevant parameters for MD process were: 1.0 L/min and 0.5 L/min for the velocities of feed solution and permeate solution, 70 °C and 25 °C for the temperatures of feed solution and permeate solution, respectively, which were the optimum conditions for M4-2 as shown in Fig. S3. The detailed membrane properties and MD performances are shown in Table 6. The averaged permeation flux of M4-2 was about 42.52 L/m^2 h during 360 min MD process with relatively obvious fluctuations (35.00–49.38 L/m^2 h), which was higher than that of commercial PTFE membrane (MPTFE-1,

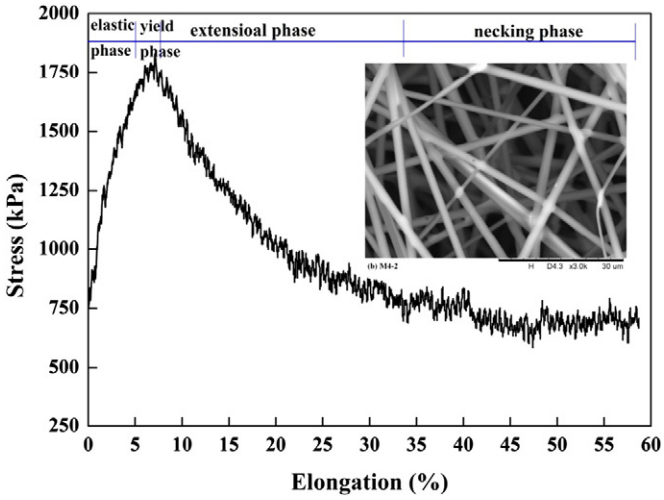

Fig. 8. Mechanical property of M4-2 and corresponding morphology of M4-2 surface.

40.93 L/m^2 h) and PVDF membrane (MPVDF, 37.19 L/m^2 h) with relatively smaller fluctuations. The main reason for this high flux might be its large pore size (8.03 μm), which made the vapor could permeate the membrane more easily with lower mass transfer resistance. The conductivity of superhydrophobic M4-2's permeate solution was 3.9 μS/cm with a conductivity variation of permeate solution (ΔC_p) of 2.3 μS/cm after 360 min test resulting in a salt rejection above 99.99%. The ΔC_ps of MPTFE-1 and MPVDF (6.7 and 4.7 μS/cm) were all higher than that of M4-2. Although the permeation flux of M4-2 was lower than that of another commercial PTFE membrane (MPTFE-2, 49.01 L/m^2 h), the ΔC_p (10.0 μS/cm) of MPTFE-2 was significantly higher than that of M4-2. These results demonstrated that membrane with superhydrophobicity (WCA > 150°) was more likely to obtain superior salt rejections than membrane with hydrophobicity (90 < WCA < 150°).

The LEP value of M4-2 (13 kPa) was significantly higher in comparison with the pressure of membrane chamber during experiment (0 kPa). This membrane LEP value was lower than the LEP values of commercial MD membranes (81–137 kPa) compared. However, a high salt rejection was still obtained during MD process which might mainly due to the superhydrophobicity of PDMS/PMMA membrane. Though pore size of M4-2 was relatively larger than the usually employed membrane pore size (<0.5 μm) for MD process, the obtained permeation flux and salt rejection efficiency were considerably impressive due to the strong water repellency and large porosity. Therefore, M4-2 is suitable for MD process, especially under free-pressure or low-pressure. These results expand the membrane selectable range for MD process remarkably, which ensures that superhydrophobic membrane with large pore size could be employed in MD process.

3.3.2. Long-term membrane distillation performance

A long-term MD process for M4-2 was conducted to investigate its actual MD evaluation as a stand-alone desalination process. The data of flux variation and conductivity variation was logged every 2 h for 32 h as shown in Fig. 9(c). The permeation flux was about 42.37 L/m^2 h during the first 12 h with a relatively stable ΔC_p (5.4 μS/cm). Although the permeation flux of M4-2 reflected a decreasing tendency from 12 h (41.62 L/m^2 h) to 24 h (33.10 L/m^2 h), this trend was relatively smooth, only about 20.8%. This flux decline indicated the pore wetting of membrane and the corresponding temperature polarization [34], therefore, the normal permeate path of vapor was blocked resulting in a lower flux than initial. The decreasing tendency became sharper and sharper after 24 h of operation. As a multiple fiber layers matrix could contain gaps or pores in each layer, M4-2 could be gradually invaded by small salt water drops when feed solution flowed through its membrane surface [35]. Therefore, pore blockage became more and more serious due

Table 5
Mechanical property of M4-2.

No.	Limiting stress (N)	Tensile strength (kPa)	Elongation at break (%)
M4-2	1.19	1833.89	58.72

to gradual pore wetting and salt invasion. The severe pore wetting and pore blockage reduced the driving force between feed and permeate sides for vapor mass transfer [34,35], which consequently brought more serious flux decline from 33.10 L/m^2 h (24 h) to 7.25 L/m^2 h (32h) as it can be seen in Fig. 9(c). The conductivity increased significantly from 12 h (6.9 μS/cm) to 32 h (90.2 μS/cm) especially after 30 h (42.8 μS/cm)

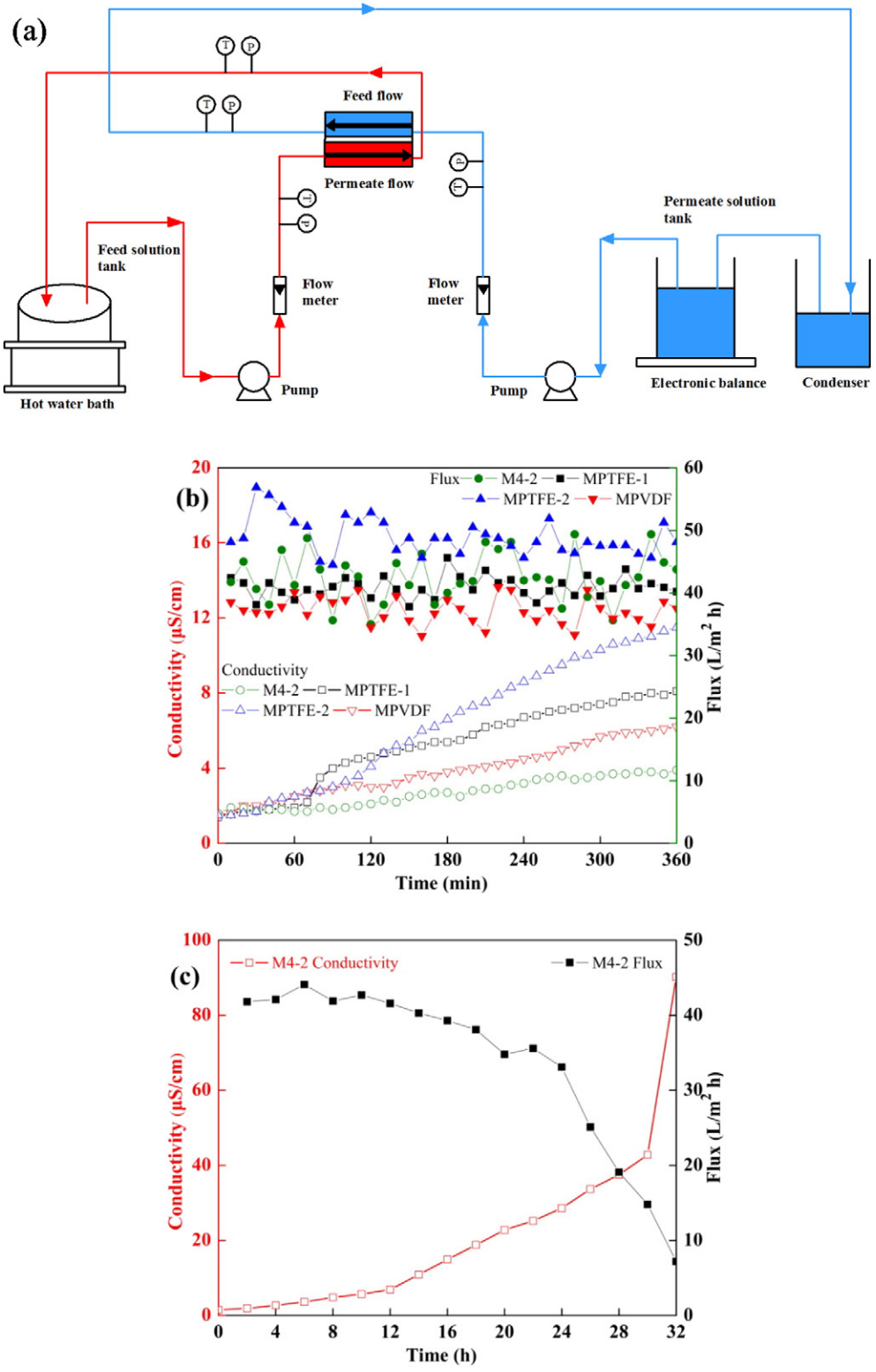

Fig. 9. (a) Schematic of membrane distillation process, (b) permeation fluxes and permeation conductivities for M4-2 and three commercial MD membranes during short-term MD process (360 min), (c) permeation flux and permeation conductivity for M4-2 during long-term MD process (32 h).

Table 6
Properties and performances of membranes used in the MD process.

No.	Properties					Performances		
	Pore size (μm)	Support material	Thickness (μm)	LEP (kPa)	WCA (°)	Flux (L/m^2 h)	ΔC (μS/cm)	Salt rejection (%)
M4-2	8.03	PET	190[a]	13	163.1 ± 3.5	42.52	2.3	99.99
MPTFE-1	0.22	PET	202	92	134.5 ± 2.8	40.93	6.7	99.98
MPTFE-2	0.45	PET	188	81	142.1 ± 0.6	49.01	10.0	99.98
MPVDF	0.45	–	104	137	124.2 ± 2.0	37.19	4.7	99.99

[a] The thickness of functional membrane was about 65.4 ± 3.4 μm, the support PET layer was about 124.6 ± 1.8 μm.

leading to an inferior salt rejection about 99.87%, and this also could be regarded as an indication for salt invasion. The yellow crystallizing on membrane after MD process and corresponding membrane WCA (121.2 ± 3.4°) as shown in Fig. S4(a) and (b) confirmed the above hypothesis of pore wetting and salt invasion. Results demonstrate this PDMS/PMMA electrospun membrane has potential to be employed in long-term (<24 h) membrane distillation application as qualified MD the membranes with considerable averaged flux of 39.61 L/m^2 h and salt rejection of 99.96%.

4. Conclusions

The results presented in this study are the first to correlate the electrospinning parameters with the properties of PDMS/PMMA electrospun membranes. Significant correlations were found between polymer concentration, voltage, injection rate and fiber diameter. Significant effect was also observed for bead formation on membrane roughness. The mass ratio 1/1/8.88/9.48 of PDMS/PMMA/THF/DMF was the best candidate for electrospinning solution system. A highest WCA of 163° could be obtained at 11 kV voltage and 0.1 mm/min injection rate under temperature of 25 °C and humidity of 35%. This high hydrophobicity was related to the surface roughness and beads structure. Obtained tensile testing results suggested that the PDMS/PMMA electrospun membrane was homogeneous-plastic material with a tensile strength of 1833.89 kPa. Considerable averaged membrane flux (39.61 L/m^2 h) and excellent salt rejection efficiency (99.96%) during 24 h MD process revealed that this novel PDMS/PMMA electrospun membrane could be a suitable candidate for desalination using membrane distillation process especially under free-pressure or low-pressure.

Abbreviation

PDMS	polydimethylsiloxane
PMMA	poly (methyl methacrylate)
DMF	*N*,*N*-dimethylformamide
THF	tetrahydrofuran
PTFE	polytetrafluoroethylene
PVDF	polyvinylidene fluoride
PET	poly (ethylene terephthalate)
WCA	water contact angle
MD	membrane distillation
DCMD	direct contact membrane distillation
TCD	tip to collector distance
SEM	scanning electron microscope
XPS	X-ray photoelectron spectroscopy
S_a	roughness average
S_q	root mean square roughness
C_f	conductivity of feed solution (mS/cm)
C_p	conductivity of permeate solution (μS/cm)
ΔC_p	conductivity variation of permeate solution during experiment

Acknowledgements

The authors gratefully acknowledge the support from the National Natural Science Foundation of China (No. 21577089) and Sinopec Zhenhai refining and chemical company.

Appendix A. Supplementary data

Supplementary data to this article can be found online at http://dx.doi.org/10.1016/j.desal.2016.11.023.

References

[1] X. Li, B. Ding, J. Lin, J. Yu, G. Sun, Enhanced mechanical properties of superhydrophobic microfibrous polystyrene mats via polyamide 6 nanofibers, J. Phys. Chem. C 113 (2009) 20452–20457.
[2] L. Zhai, F.Ç. Cebeci, R.E. Cohen, M.F. Rubner, Stable superhydrophobic coatings from polyelectrolyte multilayers, Nano Lett. 4 (2004) 1349–1353.
[3] B. Qian, Z. Shen, Fabrication of superhydrophobic surfaces by dislocation-selective chemical etching on aluminum, copper, and zinc substrates, Langmuir 21 (2005) 9007–9009.
[4] M. Ma, R.M. Hill, Superhydrophobic surfaces, Curr. Opin. Colloid Interface Sci. 11 (2006) 193–202.
[5] K. Tsujii, T. Yamamoto, T. Onda, S. Shibuichi, Super oil-repellent surfaces, Angew. Chem. Int. Ed. Engl. 36 (1997) 1011–1012.
[6] B. Ding, T. Ogawa, J. Kim, K. Fujimoto, S. Shiratori, Fabrication of a super-hydrophobic nanofibrous zinc oxide film surface by electrospinning, Thin Solid Films 516 (2008) 2495–2501.
[7] W. Cui, X. Li, S. Zhou, J. Weng, Investigation on process parameters of electrospinning system through orthogonal experimental design, J. Appl. Polym. Sci. 103 (2007) 3105–3112.
[8] A. Frenot, I.S. Chronakis, Polymer nanofibers assembled by electrospinning, Curr. Opin. Colloid Interface Sci. 8 (2003) 64–75.
[9] S. Agarwal, A. Greiner, J.H. Wendorff, Functional materials by electrospinning of polymers, Prog. Polym. Sci. 38 (2013) 963–991.
[10] M. Jin, X. Feng, J. Xi, J. Zhai, K. Cho, L. Feng, L. Jiang, Super-hydrophobic PDMS surface with ultra-low adhesive force, Macromol. Rapid Commun. 26 (2005) 1805–1809.
[11] B. Cortese, S. D'Amone, M. Manca, I. Viola, R. Cingolani, G. Gigli, Superhydrophobicity due to the hierarchical scale roughness of PDMS surfaces, Langmuir 24 (2008) 2712–2718.
[12] M. Xiao, J. Zhou, Y. Zhang, X. Hu, S. Li, Pertraction performance of phenol through PDMS/PVDF composite membrane in the membrane aromatic recovery system (MARS), J. Membr. Sci. 428 (2013) 172–180.
[13] M. Nour, K. Berean, A. Chrimes, A.S. Zoolfakar, K. Latham, C. McSweeney, M.R. Field, S. Sriram, K. Kalantar-zadeh, J.Z. Ou, Silver nanoparticle/PDMS nanocomposite catalytic membranes for H2S gas removal, J. Membr. Sci. 470 (2014) 346–355.
[14] B.-H. Jo, L.M. Van Lerberghe, K.M. Motsegood, D.J. Beebe, Three-dimensional microchannel fabrication in polydimethylsiloxane (PDMS) elastomer, J. Microelectromech. Syst. 9 (2000) 76–81.
[15] Y. Liu, D. Yang, T. Yu, X. Jiang, Incorporation of electrospun nanofibrous PVDF membranes into a microfluidic chip assembled by PDMS and scotch tape for immunoassays, Electrophoresis 30 (2009) 3269–3275.
[16] D. Yang, X. Liu, Y. Jin, Y. Zhu, D. Zeng, X. Jiang, H. Ma, Electrospinning of poly (dimethylsiloxane)/poly (methyl methacrylate) nanofibrous membrane: fabrication and application in protein microarrays, Biomacromolecules 10 (2009) 3335–3340.
[17] K. Matabola, R. Moutloali, The influence of electrospinning parameters on the morphology and diameter of poly (vinyledene fluoride) nanofibers-effect of sodium chloride, J. Mater. Sci. 48 (2013) 5475–5482.
[18] A. Alkhudhiri, N. Darwish, N. Hilal, Membrane distillation: a comprehensive review, Desalination 287 (2012) 2–18.
[19] B.S. Lalia, E. Guillen-Burrieza, H.A. Arafat, R. Hashaikeh, Fabrication and characterization of polyvinylidenefluoride-co-hexafluoropropylene (PVDF-HFP) electrospun membranes for direct contact membrane distillation, J. Membr. Sci. 428 (2013) 104–115.

[20] L.D. Tijing, J.-S. Choi, S. Lee, S.-H. Kim, H.K. Shon, Recent progress of membrane distillation using electrospun nanofibrous membrane, J. Membr. Sci. 453 (2014) 435–462.
[21] Z.-Q. Dong, X.-h. Ma, Z.-L. Xu, W.-T. You, F.-b. Li, Superhydrophobic PVDF–PTFE electrospun nanofibrous membranes for desalination by vacuum membrane distillation, Desalination 347 (2014) 175–183.
[22] S. Rosa, J. Crespo, A. Meléndez, J. Santiago-Avilés, I. Ramos, E. Campo, CNT dispersion and precursor synthesis for electrospinning of polymer-CNT composites, SPIE NanoScience + Engineering, International Society for Optics and Photonics, 2011 (81070L-81070L-81076).
[23] S. Aerts, A. Vanhulsel, A. Buekenhoudt, H. Weyten, S. Kuypers, H. Chen, M. Bryjak, L. Gevers, I. Vankelecom, P. Jacobs, Plasma-treated PDMS-membranes in solvent resistant nanofiltration: characterization and study of transport mechanism, J. Membr. Sci. 275 (2006) 212–219.
[24] S.B. Amor, G. Baud, M. Jacquet, G. Nanse, P. Fioux, M. Nardin, XPS characterisation of plasma-treated and alumina-coated PMMA, Appl. Surf. Sci. 153 (2000) 172–183.
[25] P.-G. De Gennes, F. Brochard-Wyart, D. Quéré, Capillarity and Wetting Phenomena: Drops, Bubbles, Pearls, Waves, Springer Science & Business Media, 2013.
[26] N. Nuraje, W.S. Khan, Y. Lei, M. Ceylan, R. Asmatulu, Superhydrophobic electrospun nanofibers, J. Mater. Chem. A 1 (2013) 1929–1946.
[27] K. Lee, H. Kim, H. Bang, Y. Jung, S. Lee, The change of bead morphology formed on electrospun polystyrene fibers, Polymer 44 (2003) 4029–4034.
[28] H. Fong, I. Chun, D. Reneker, Beaded nanofibers formed during electrospinning, Polymer 40 (1999) 4585–4592.
[29] A. Razmjou, E. Arifin, G. Dong, J. Mansouri, V. Chen, Superhydrophobic modification of TiO 2 nanocomposite PVDF membranes for applications in membrane distillation, J. Membr. Sci. 415 (2012) 850–863.
[30] M. Ghiasi, E. Naghashzargar, D. Semnani, Silk fibroin nano-coated textured silk yarn by electrospinning method for tendon and ligament scaffold application, Nano Hybrids, Trans Tech Publ 2014, pp. 35–51.
[31] C.J. Buchko, L.C. Chen, Y. Shen, D.C. Martin, Processing and microstructural characterization of porous biocompatible protein polymer thin films, Polymer 40 (1999) 7397–7407.
[32] X. Mo, C. Xu, M. Kotaki, S. Ramakrishna, Electrospun P (LLA-CL) nanofiber: a biomimetic extracellular matrix for smooth muscle cell and endothelial cell proliferation, Biomaterials 25 (2004) 1883–1890.
[33] W. Zuo, M. Zhu, W. Yang, H. Yu, Y. Chen, Y. Zhang, Experimental study on relationship between jet instability and formation of beaded fibers during electrospinning, Polym. Eng. Sci. 45 (2005) 704–709.
[34] M.M.A. Shirazi, A. Kargari, M. Tabatabaei, Evaluation of commercial PTFE membranes in desalination by direct contact membrane distillation, Chem. Eng. Process. Process Intensif. 76 (2014) 16–25.
[35] Y. Liao, R. Wang, M. Tian, C. Qiu, A.G. Fane, Fabrication of polyvinylidene fluoride (PVDF) nanofiber membranes by electro-spinning for direct contact membrane distillation, J. Membr. Sci. 425–426 (2013) 30–39.